Experiments in Fluids 31 (2001) 519–532 © Springer-Verlag 2001

Flow analysis of two-dimensional pulsed jets by particle image velocimetry

J. C. Béra, M. Michard, N. Grosjean, G. Comte-Bellot

Abstract A purely alternating jet without mean mass flux and a mixed pulsed jet containing an additional blowing component were investigated by particle image velocimetry (PIV). The jets issued from a two-dimensional slit connected to a converging nozzle, opening normally from a flat wall. The pulsation was driven by a loudspeaker. The mean velocity fields were characterized by the combination of downstream directional blowing and omni-directional suction. The velocity fluctuations were dominated by contra-rotating eddy pairs synchronized with the pulsation and formed at the jet edges during blowing. Phase-synchronized measurements permit the investigation of the averaged patterns and the cycle-to-cycle fluctuations of these vortices. The mean trajectories of vortex centers during a whole injection cycle show how large lateral jet expansions are achieved. For a *purely alternating jet*, the expansion takes place close to the slit. For a *mixed pulsed jet*, the vortices develop farther from the orifice. In addition, proper orthogonal mode decomposition demonstrates that only a few modes are required to represent the main events of the flow dynamics.

1 Introduction

From the time that Crow and Champagne (1971) investigated the orderly structure of turbulent jets, the dynamics of pulsed jets has generated great interest among the scientific community. A possible increase of the jet entrainment rate was the main advantage. Several experiments on circular jets were done by Binder et al. (1971, 1972), Curtet and Girard (1973), Bremhorst and Harch (1979) and Bremhorst and Watson (1981). In industrial applications, pulsed jets have been widely used in internal combustion engines in order to improve the mixing between fuel and air (Heywood 1988).

More recently, pulsed jets have been discovered as efficient actuators for flow control. The unsteady aspect was so important that in some experiments the continuous component of the pulsed jet has been even suppressed – hence some suction effects were added. The separation of boundary layers on cylinders or wings could be delayed, hence generating lift, with actuators located at the wall underneath the flow. Eventually, this approach would permit the improvement of the flight response of aircraft without geometry changes of wing profiles. For cylinders, the case of laminar boundary layers has been investigated by Amitay et al. (1997), and the case of turbulent separation by Béra et al. (1998). For airfoil wings, most of the research has been so far done by Seifert et al. (1993), MacManus and Magill (1997) and Greenblatt et al. (1998). Pioneering works on flow control in moderate and large-angle diffusers have been conducted by Kwong and Dowling (1994) and Ben Chiekh et al. (2000) in order to increase the mixing, to raise the mean pressure recovery and to reduce pressure oscillations.

Understanding the physical mechanisms involved in the interactions between pulsed jets and external flow has also been a developing topic. The dye visualization of vortex rings evolving over a flat plate in a cross-flow by Chang and Vakili (1995) provided the first elements of the vortex deformation at extremely low speed. At higher speeds, Wygnanski (1997) suggested that separation can be delayed over an airfoil flap when active eddies, which are introduced into the flow, are able to manipulate the free shear layer so as to accompany it downstream to the flap trailing edge. Using particle image velocimetry (PIV), Béra et al. (2000) showed that pulsed jets affect flow separation on a cylinder by reaching the separated layer, generating strong vortices of the same sign as the shear induced by the external flow and bringing fluid close to the cylinder wall. McManus and Magill (1997) found that 45° skew oblique jets were more active than jets normal to the wall because of a stronger coupling with the inclined structures constituting turbulent boundary layers. Numerical predictions have also attempted to analyze the control process, e.g. the unsteady RANS approach of Hassan and Janakiram (1997) for a NACA airfoil, the unsteady $k-\varepsilon$ simulations of Getin (2000) for a cylinder and the LES simulations of Mary et al. (2000) also for a cylinder. In all these cases, refined meshes are needed across the jet exit, and the unsteady feature is the hardest part to simulate.

In that context, the simple case of a pulsed jet without external flow has very recently received further attention. It constitutes a separate and entire benchmark for numerical studies as well as for experimental investigations, because of a wide range of both injector and flow

Received: 10 August 1999 / Accepted: 10 January 2001

J. C. Béra (✉), M. Michard, N. Grosjean, G. Comte-Bellot
Laboratoire de Mécanique des Fluides et d'Acoustique
Ecole Centrale de Lyon, CNRS UMR 5509, GDR 1186
BP 163, F-69131 Ecully cedex, France
e-mail: Jean-Christophe.Bera@ec-lyon.fr
Fax: +33-4-72189143

This study was supported by the French Government (DGA – SPAé). The technical assistance of Laurent Graftieaux has been very useful.

parameters that govern the jet development. These include the Reynolds numbers of the injection, the Strouhal number of the pulsation, the relative stroke-length, the shape of the velocity profile at the jet exit (top-hat when the pulsed jets are issued from a converging nozzle or with a distributed vorticity, and additional unsteadiness when pulsed jets issue from cavities with inner sharp angles and long connection ducts). For example, Redionitis et al. (1999) and Smith et al. (1999) mostly investigated the Reynolds and Strouhal effects. The DNS simulations of Rizetta et al. (1998) and Lee and Goldstein (2000) extensively examined the cavity, including the shape of the slit lips. Furthermore, the time–velocity injection cycle function is an important parameter as pointed out by Kral et al. (1997), who modeled 10 cases of pulsed jets, not yet all completely compared with experiments. More numerical data were provided by Getin (2000).

The present experimental study focused on the comparison between two typical cases of injection: *purely alternating injection with zero mass net flux* – also called synthetic jet – and *mixed pulsed injection* with fully pulsed blowing, and hence a continuous mean flow. The injection was made through a convergent nozzle in order to have well-defined spatial velocity conditions at the orifice. This technology was used extensively by Sunyach and Béra at our institution for flow control. The Reynolds and Strouhal numbers based on the peak velocity, the orifice width and the forcing frequency were $\mathrm{Re} = 1300$, and $\mathrm{St} = 0.10$. These were close to the values met in the synthetic jets issued from rectangular cavities representative of MEMS piezoelectric technology, as developed by Seifert et al. (1993), Amitay et al. (1997) and Smith and Glezer (1998). For the experimental technique, we have selected particle image velocimetry (PIV), which permits instantaneous velocity maps of the whole flow to be obtained. Software processing then gave access to phase-averaged maps that provided the key dynamic flow features. The large-scale structures generated by the alternating injection could therefore be observed during their downstream evolution, concomitantly with the flow changes existing near the injection nozzle. Finally, PIV permitted us, through the very productive snapshot technique of the proper orthogonal decomposition (POD), to investigate the cyclic variation of the vortices generated during blowing.

The organization of the paper is as follows: the experimental set-up is described in Sect. 2, with the actuator characteristics and the PIV features. Results dealing with the velocity profiles and the kinetic energy values are given in Sect. 3. Some self-similarity considerations are discussed in Sect. 4, mostly concerning the lateral rate of expansion of the various jets. Conditional phase statistics including POD results are presented in Sect. 5, as well as vortex trajectories for the most significant cases.

2
Experimental set-up

2.1
Jet generation

All jets investigated issued from the same longitudinal slit, 100 mm long, $e = 1$ mm wide, mounted in a flat plate. The

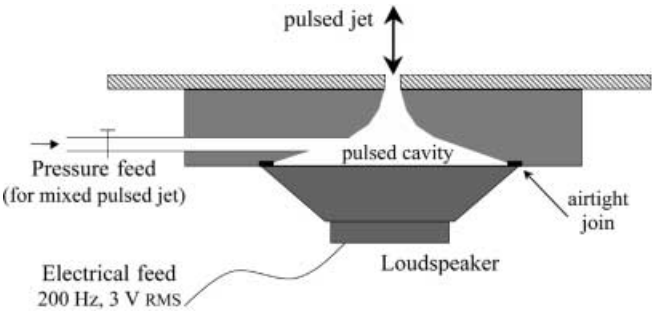

Fig. 1. Sketch of pulsed jet generator

experiments were carried out in a large room with ambient air at rest. Two kinds of unsteady blowing jets were explored: a *purely alternating jet* and a *mixed pulsed jet* with both alternating and continuous injections.

The *purely alternating jet* issued from a convergent nozzle tightly fitted to the rim of a loudspeaker, as shown in Fig. 1. The slit was perpendicular to the flat wall, and the orifice edges were sharp. The pressure fluctuation was sinusoidal at a frequency of 200 Hz. The loudspeaker was fed by a 3 V RMS voltage, generating velocity fluctuations of approximately 14 m/s RMS at the aperture.

The *mixed pulsed jet* injection was based on the same actuator as the purely alternating jet, except that a constant pressure feed was added to generate an overpressure in the pulsed cavity. This feed was adjusted to suppress the suction phase: at the minimal value of the injection cycle, the velocity at the slit exit was approximately zero.

For comparison, two classical *steady blowing jets* were generated through the same injector by only the constant overpressure in the cavity. The jet exit velocities were: 10 m/s (low blowing) giving the same mean velocity as the purely alternating jet at $X = 30$ mm from the slit; and 20 m/s (high blowing) generated by the same constant pressure feed as that used in the mixed pulsed jet. A constant underpressure, or depression, in the cavity was also tested to study the effect of a *continuously sucking* slit. This basic case is important as it corresponds to half a cycle in a purely alternating jet.

The time trace of the instantaneous velocity cycle at the slit exit center was acquired by hot-wire measurements for every injection studied. Figure 2 shows these injection cycles.

2.2
PIV measurements

Figure 3 shows the set-up used for the PIV measurements. The view plane was normal to the slit at the mid-span of the slit. Figure 3 also gives the definition of the coordinate axes. The observation field was 35 mm × 35 mm, and the jet slit opened at $X = Y = 0$.

The measurements were carried out with a Dantec system. Two coupled YAG laser sources (300 mJ Quantel lasers) provide pairs of laser pulses at a synchronizable frequency of about 10 Hz. The time delay between pulses was 30 μs. The visualization light sheet was 0.3 mm in width. The flow was seeded with micrometer-sized droplets generated by a smog generator. Droplets were atomized in the surrounding fluid before every experiment. Afterwards, the alternating blowing and suction ensured the flow to be

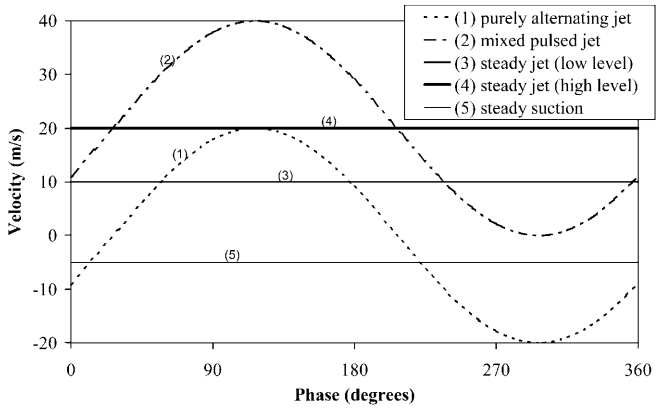

Fig. 2. Injection cycle for jets investigated

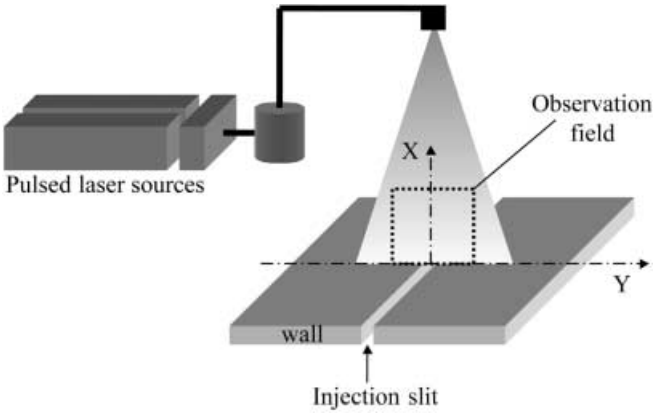

Fig. 3. Principle of PIV measurements

correctly seeded, even near the slit. The light scattered by droplets during laser illuminations was recorded with a CCD Kodak Megaplus E.S. 1.0 camera. The magnification ratio was 1/3. The 1008×1018 pixels images were processed using cross-correlation. The interrogation window was fixed to 32×32 pixels, providing a spatial resolution of approximately 1 mm $\times$ 1 mm. The overlap ratio between adjacent interrogation windows was 50%, providing instantaneous velocity fields with 63×63 vectors.

2.3
PIV data processing

For the steady jets, the mean and fluctuating velocities were computed by ensemble averaging performed over a set of 990 instantaneous fields. For the pulsed jets, the PIV measurements could be triggered by logic signals synchronized with the electric supply of the loudspeaker. For a given phase in the injection cycle, phase-average velocity fields were obtained by averaging 55 instantaneous velocity fields. The whole cycle was covered by 18 phases regularly spaced, including blowing and suction. Therefore, a total set of 990 instantaneous samples was available for time-averaged computations. It was verified that the mean of the 18 phase-averages was compatible with the mean of random acquisitions.

The pulsed jet generates vortices during blowing, as already established by the visualizations of Smith and Glezer (1998) in the case of purely alternating jets. The

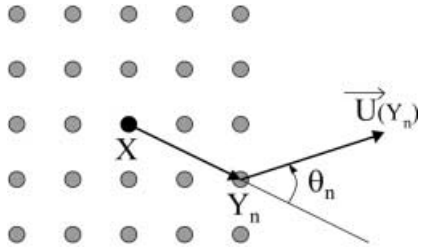

Fig. 4. Integration domain for vortex Γ-criterion calculation at any point X

vortex centers are localized, using the topological criterion developed by Michard et al. (1997). At each location $\vec{X}$ in the flow (Fig. 4) the dimensionless function $\Gamma(\vec{X}) = \frac{1}{S}\int_{\vec{y}\in S} \sin\theta \, dS$ was obtained, where S is a domain surrounding $\vec{X}$ and θ is the angle between $\vec{Y} - \vec{X}$ and the velocity $\vec{U}(\vec{Y})$. The value of $\Gamma(\vec{x})$ varies in the range -1 to 1, and the vortex center $\vec{X}$ corresponds to $\Gamma(\vec{X}) \approx 1$ (counter clockwise rotation) or $\Gamma(\vec{X}) \approx -1$ (clockwise rotation). The vortex centers could be obtained for every one of the 55 instantaneous velocity fields taken at a given phase. Fluctuations of the phase-average vortex center around the mean position could therefore be also investigated.

POD was implemented on the series of 55 phase-synchronized velocity fields, using the snapshot method (Sirovich 1987). The spatial modes were deduced from the eigenvalues and eigenvectors of the cross-correlation matrix between snapshots.

3
Maps of the flow statistics

3.1
Maps of mean velocity fields

The averaged velocity fields for the different injections are shown in Fig. 5. A relatively good symmetry of the fields with respect to the injection plane can be observed. However, a slight jet deviation toward the right is perceptible, due to molding imperfection of the nozzle. This deviation will be corrected for when analyzing the mean velocity profiles in Sect. 4. Close to the slit, the PIV spatial resolution does not permit precise observation of the jet exit, as the 1 mm slit width is of the order of the PIV interrogation window. There is bias due to excessively strong velocity gradients and excessively large particle displacements. For the high-level steady and mixed jets, the measured mean velocities were therefore systematically too small in the potential jet region and its mixing layers (roughly $X/e < 5$ and $|Y|/e < 1$). Of course, we could have used a bigger nozzle width as in the experiments by Smith et al. (1999), but our intent was to investigate precisely the same experiments that were embedded in our flow control experiments (Béra and Sunyach 1998, Michard et al. 1998).

The basic *steady* fields (*blowing* and *suction*) provide two different flow structures. On the one hand (Fig. 5a), *steady blowing* generates a classical jet normal to the wall, with regular spreading and entrainment of the surrounding fluid. On the other hand (Fig. 5b), *steady suction*

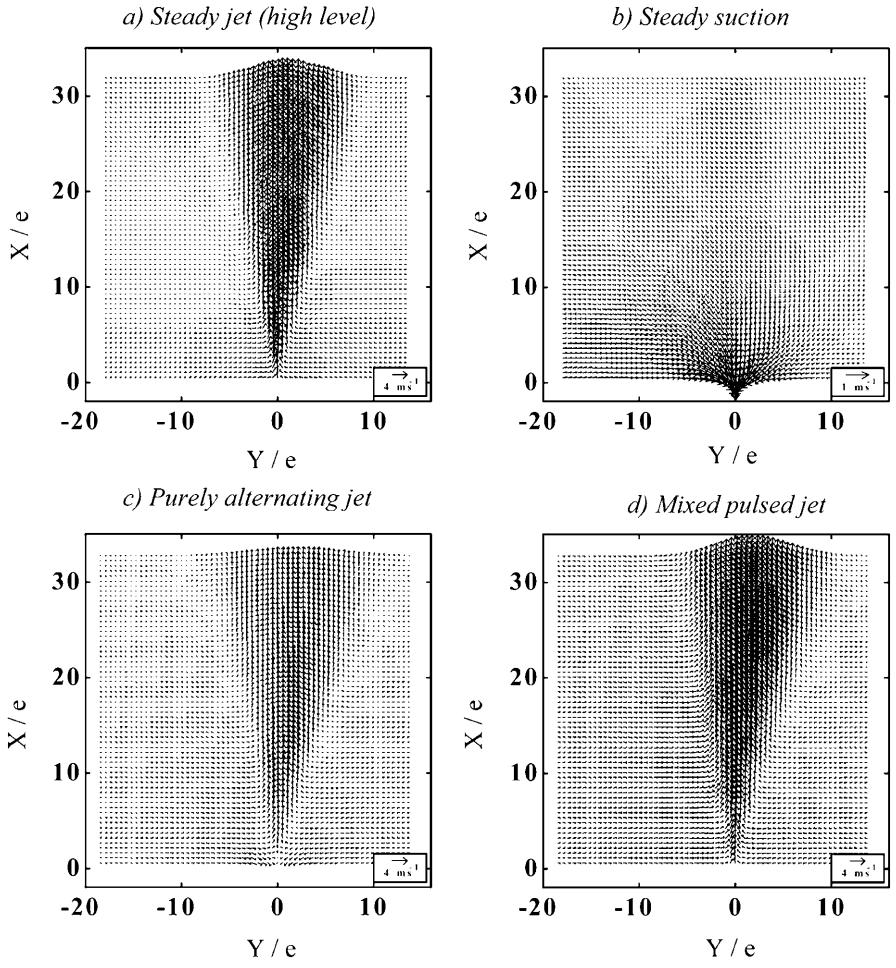

Fig. 5a–d. Mean velocity fields: **a** Steady jet (high level), **b** Steady suction, **c** Purely alternating jet, **d** Mixed pulsed jet

generates an omnidirectional velocity field toward the slit. In particular, tangential in-flow is visible on either side of the slit close to the wall.

Figure 5c shows that the *purely alternating jet* generates a mean flow, even without mean mass flux introduced at the nozzle. Indeed, during the blowing phase, the fluid is pushed away from the nozzle sufficiently far downstream so that it can later escape from the suction imposed at the nozzle. Of course, the resulting mean flow structure is different from that of a classical steady jet. The mean velocity on the jet centerline shows a saddle point (at $X/e = 2$) where the mean effect of suction compensates for the mean effect of blowing. Above the saddle point, the mean velocity field looks like that of a classical steady blowing jet, except that the aerodynamic driving effect of the pulsed jet is very intense.

The mean flow of the *mixed pulsed jet* (Fig. 5d) resembles that of the steady jet of the same mean injection (Fig. 5a). However, the lateral entrainment is more intense, with larger velocity magnitudes, showing clearly that the pulsation ultimately results in an acceleration of the mean jet.

3.2
Maps of fluctuating kinetic energy

The maps of the fluctuating kinetic energy fields given in Fig. 6 confirm the great disparity between the different types of jets. Of course, the steady suction is not considered because the flow is laminar.

Figure 6a–b concern the *low-* and *high-level steady jet*s. The kinetic energy maps show elongated contours in the downstream direction, which reflects the lateral diffusion associated with the longitudinal convection. The mean jet width obtained at the downstream distance of $X/e = 35$ is of the same order for both blowing levels, which is consistent with the expected jet similarity.

Figure 6c deals with the *purely alternating jet*. The iso-kinetic energy contours now have a large transverse (cross-stream-wise) expansion, from very close to the nozzle up to around $X/e = 10$; afterwards, the jet expansion is reduced. The high fluctuations when X/e is around 10 are attributed to the periodic entrainment of the surrounding fluid, as will be made clear in Sect. 5. Further downstream, the fluctuating levels reduce, so that lateral expansion cannot proceed further.

Figure 6d concerns the *mixed pulsed jet*. A large transverse expansion is now observed between $X/e = 3$ to $X/e = 15$ from the slit. Afterwards, the expansion rate is reduced as for the purely alternating jet. The iso-fluctuation lines present some similarity with those of the alternating jet, but they essentially differ from them in that an additional downstream convection exists due to the steady part of the injection. In terms of fluctuation magnitudes, the mixed pulsed jet generates larger fluctuating kinetic

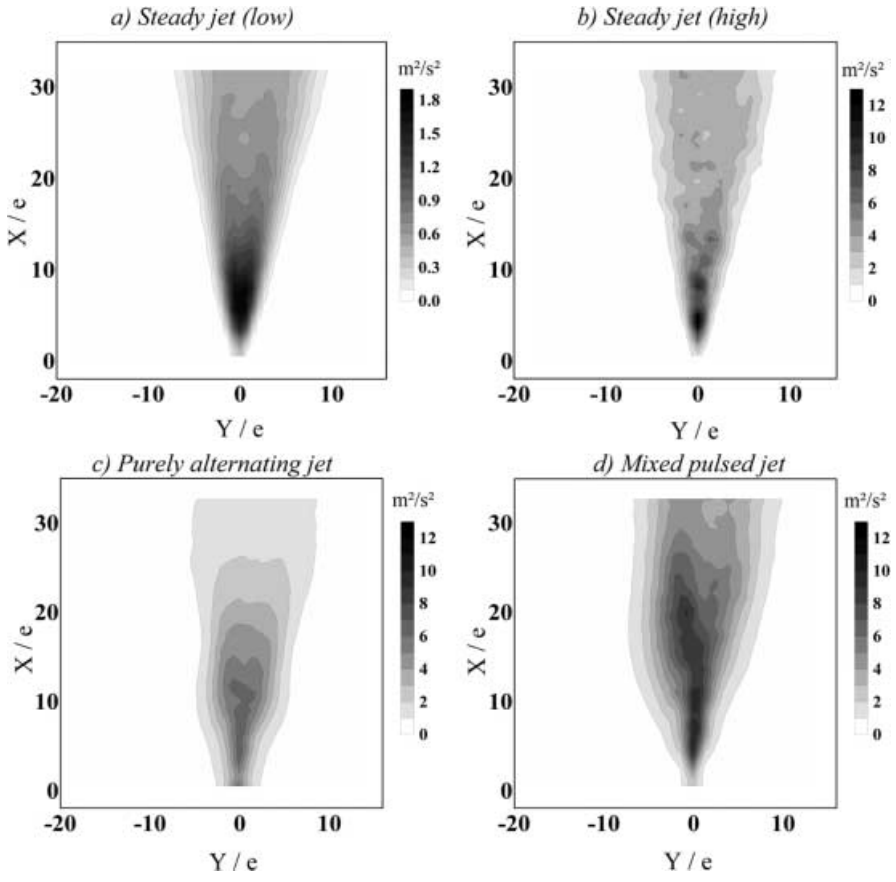

Fig. 6a–d. Kinetic energy of velocity fluctuations: **a** Steady jet (low), **b** Steady jet (high), **c** Purely alternating jet, **d** Mixed pulsed jet

energy levels than either the purely alternating jet or the steady blowing, around as much as the sum of both. Let us recall that mixed injection has been selected precisely to be the sum of the pure alternating injection and the high-level steady injection, compare with Fig. 2.

4
Self-similarity approach of the velocity profiles

4.1
Maximum velocity and half-width of the jets

In order to compare the different flow structures, we focus on velocity profiles in the usual similarity coordinates, using X/e, Y/b and U/U_m. The half-width b is defined as the lateral distance at which the mean jet profile is reduced to half of its maximum velocity U_m at the same axial section. The same definition has been used for the three kinds of injection investigated: *steady blowing jet, purely alternating jet* and *mixed pulsed jet*. In all the plots, we will only consider axial distances $X/e > 5$, consistent with our PIV measurement accuracy.

The jet half-width b/e is shown in Fig. 7 as a function of the distance from the slit. The steady injection provides an identical expansion for both blowing levels, with the usual linear increase. The spreading of the purely alternating jet is higher than that of a steady jet at all distances from the nozzle. Moreover, a sharp increase of b/e occurs for $X/e > 15$, in accordance with the hot-wire experimental curve of Smith et al. (1999). As an interesting point, the mixed pulsed jet gives an intermediate curve between the two previous types of jets: indeed, b/e seems to collapse with the alternating jet up to $X/e = 15$, and with the steady blowing above $X/e = 20$.

Figure 8 shows the jet maximum velocity U_m as a function of X/e. For steady blowing we obtain the usual decreasing law, whatever the blowing level. In terms of a power law, the exponent is −0.40 and close to the theoretical value of −0.50. For the purely alternating jet, U_m increases from zero at the slit to a maximum around $X/e = 12$, and then slowly decreases. Smith and Glezer (1998) also found a maximum located around $X/e = 8$, and

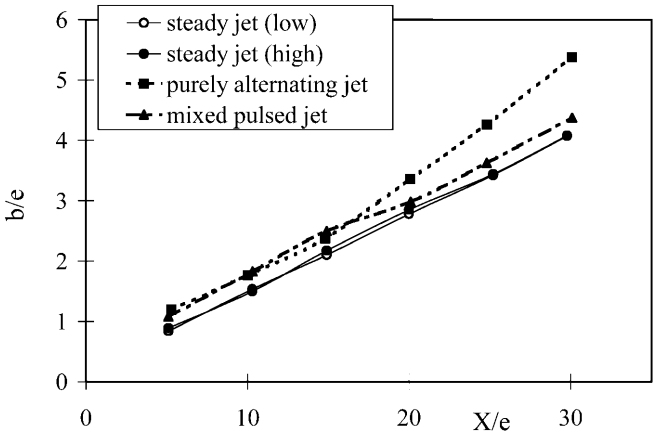

Fig. 7. Half-width of the jet as a function of distance from injection nozzle

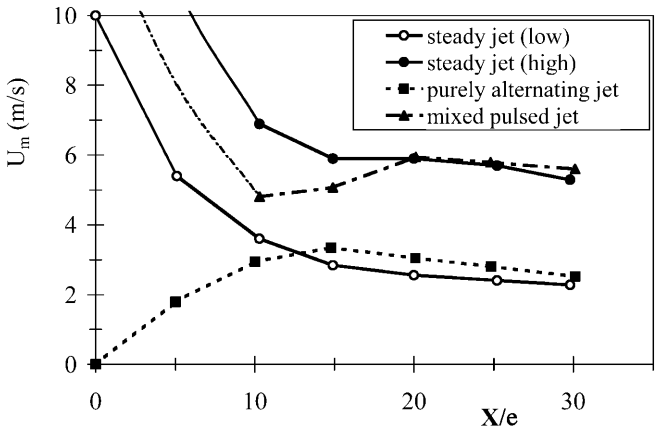

Fig. 8. Maximum jet velocity as a function of distance from injection nozzle

Kral et al. (1997) predicted it around $X/e = 10$. For the mixed pulsed injection, the evolution of U_m with X/e is more complex because of the presence of an intermediate minimum. This behavior can be also observed in the predictions made by Kral et al. (1997) – case T6.

4.2
Mean velocity profiles

The mean velocity profiles are shown in Fig. 9. In every X/e section, the slight asymmetry of the PIV profiles observed in Fig. 5 was corrected by bringing the U_m position onto the Y-axis, i.e. $Y = 0$ at the jet centerline.

For the steady blowing jets, all the stream-wise velocity profiles U/U_m collapse satisfactorily (Fig. 9a–b, left). The cross-stream velocity profiles V/U_m reach similarity slightly farther downstream (Fig. 9a–b, right). The V components are directed outwards when Y/e is small, the flow being dominated by the decrease of the mean longitudinal velocity near the jet centerline, and inwards when Y/e is large, corresponding to the entrainment of surrounding fluid.

In the case of the purely alternating jet, see Fig. 9c, the similarity of the mean longitudinal velocity profiles is surprisingly good. A specific feature, however, is the presence of negative U/U_m velocities for $|Y|/b \geq 2$. This indicates that large rotating secondary flows are associated with the entrainment effects that exist in the surrounding fluid. The mean cross-stream velocity profiles V/U_m are far from similarity. Moreover, for $X/e = 5$ and 10, V/U_m have very large magnitudes, with profiles showing only entrainment effects and no jet lateral expansion. Indeed, the blowing phase brings inward contributions toward the slit by jet entrainment, and the suction phase does the same by direct aspiration.

The mixed pulsed jet (Fig. 9d) presents some similarity with the alternating pulsed jet. At large Y/b, negative values of U/U_m are present, but less pronounced. These negative values appear farther downstream from the nozzle because of convection by the mean blowing component. The V/U_m profiles behave, regarding the surrounding fluid entrainment, as an intermediate case between the steady injection and the alternating injection.

Fig. 9a–d. Mean velocity normalized profiles, ○ $X/e = 5$, □ $X/e = 10$, Δ $X/e = 15$, ◇ $X/e = 20$, ● $X/e = 25$, ■ $X/e = 30$: **a** Steady jet (low level), **b** Steady jet (high level), **c** Purely alternating jet, **d** Mixed pulsed jet

4.3
Profiles of the RMS velocity fluctuations

The relative intensity of the stream-wise and cross-stream velocity fluctuations, u'/U_m and v'/U_m, are presented in Fig. 10.

The low-level steady blowing provides perfect similarity profiles almost as soon as $X/e = 15$ (Fig. 10a). The conventional patterns are retrieved with the usual dip on the jet axis for u'/U_m. At high blowing levels, the similarity is a little less marked (Fig. 10b), but as a whole, the normalized profiles do not depend on the blowing injection level.

Now for the alternating jet (Fig. 10c), both the u'/U_m and v'/U_m profiles need large values of X/e, around $X/e = 25$, to show similarity. In addition, the intensity values on the jet centerline are much higher than in the case of a steady jet: $u'/U_m \approx 0.40$ and $v'/U_m \approx 0.35$ – versus 0.25 and 0.20, respectively, for steady blowing. This fact, added to the increased lateral expansion observed in Fig. 7, shows that a specific flow pattern is now present.

The mixed jet profiles (Fig. 10d), present similitude only when $X/e > 20$. Then the u'/U_m and v'/U_m values are close to those obtained for steady blowing.

5
Identification of the large-scale structures generated by pulsation

5.1
Phase-average velocity fields

Phase-average velocity fields are measured in the case of the purely alternating jet (Figure. 11) and the mixed pulsed jet (Fig. 12). These measurements illustrate the presence of pairs of contra-rotating eddies, which develop and move downstream over the injection cycle.

The results for phase 0°, which corresponds to the end of suction (see Fig. 2), are presented in the first vector field of Figs. 11 and 12. They show that alternating injection favors the separation of the vortices generated by the previous blowing. These vortices are around $X/e = 15$ for the purely alternating jet and $X/e = 25$ for the mixed pulsed jet. For the purely alternating jet, the separation is clearly marked by a saddle point in front of the injection slit at approximately $X/e = 5$ from the nozzle. The horizontal partition line $\{X/e = 4\}$ delimits the lower zone where the fluid is aspirated by the slit, and the upper zone where the flow is governed by an autonomous pair of ejected contra-rotating eddies. For the mixed pulsed jet, the separation cannot be localized because of the continuous blowing component. In both cases the pairs of contra-rotating eddies are continuously moving away from the wall.

The phases 60–120–180°, which correspond to blowing, are given in the 2nd, 3rd and 4th vector fields of Figs. 11 and 12. The birth of the contra-rotating eddies is clearly visible close to the nozzle. Farther downstream the previous pair continues its evolution, pushed also by the directional blowing imposed at the slit.

a) Steady jet (low level)

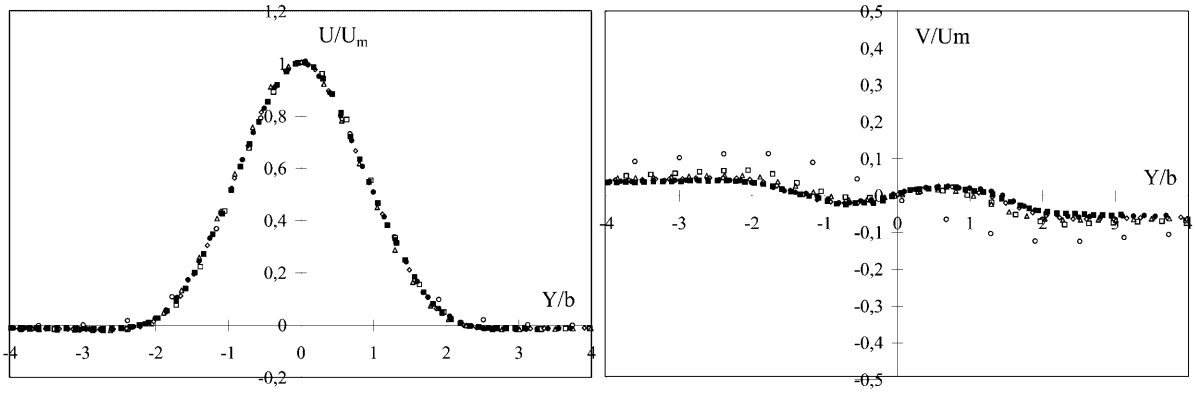

b) Steady jet (high level)

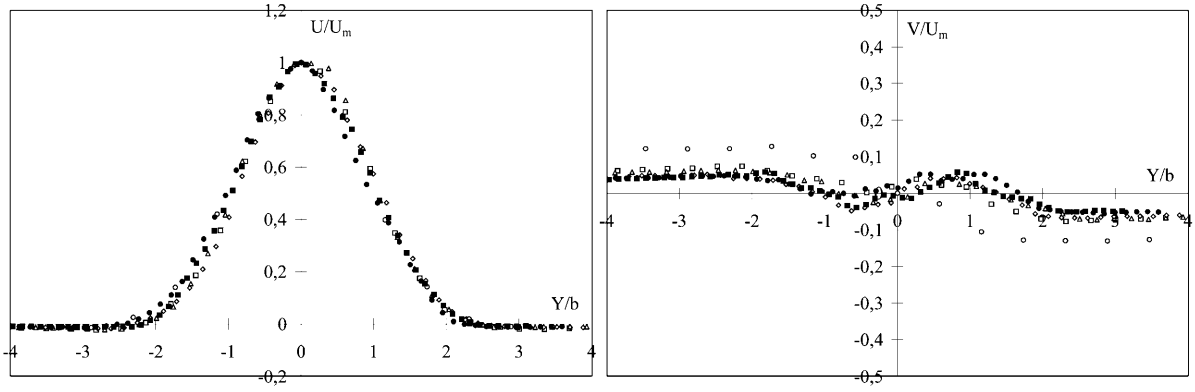

c) Purely alternating jet

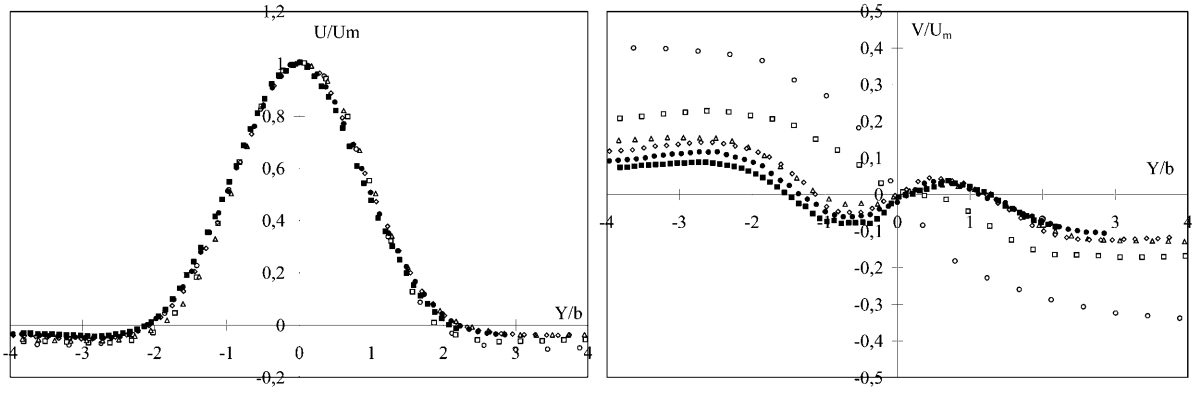

d) Mixed pulsed jet

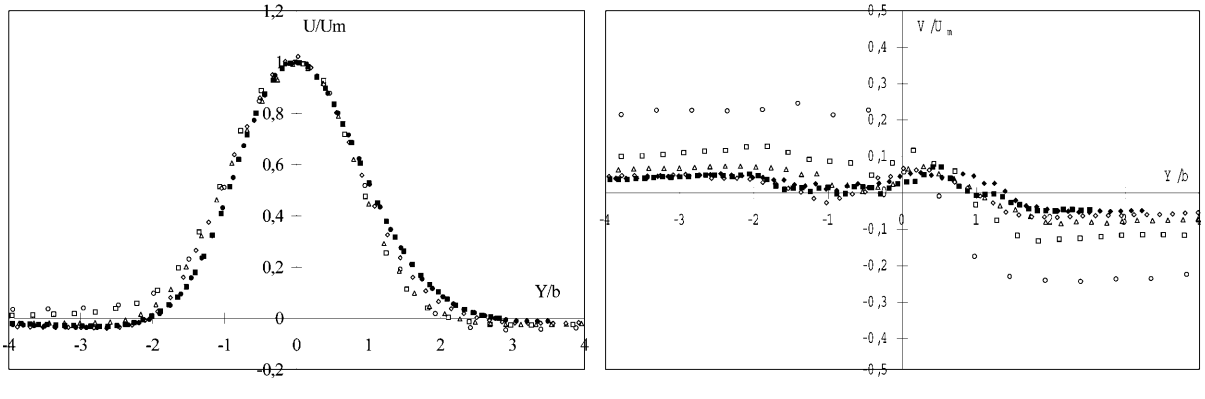

a) Steady jet (low level)

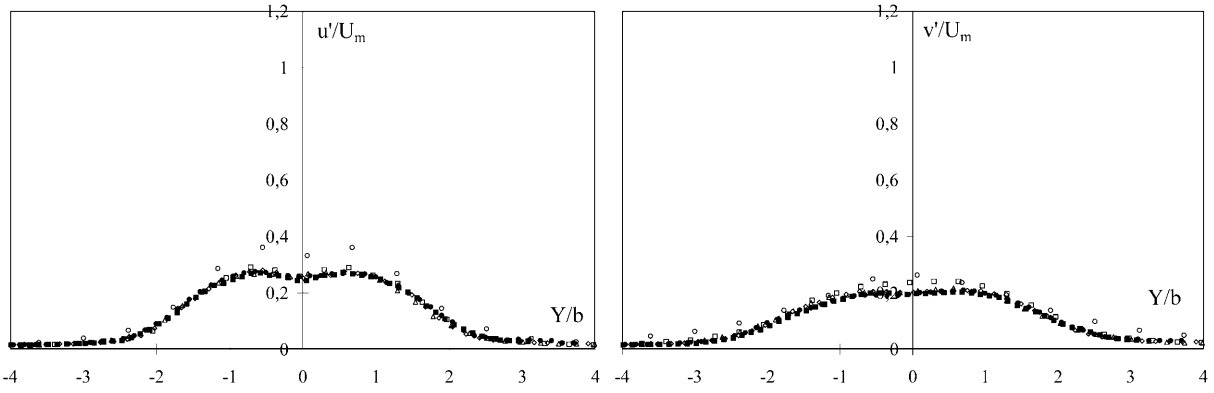

b) Steady jet (high level)

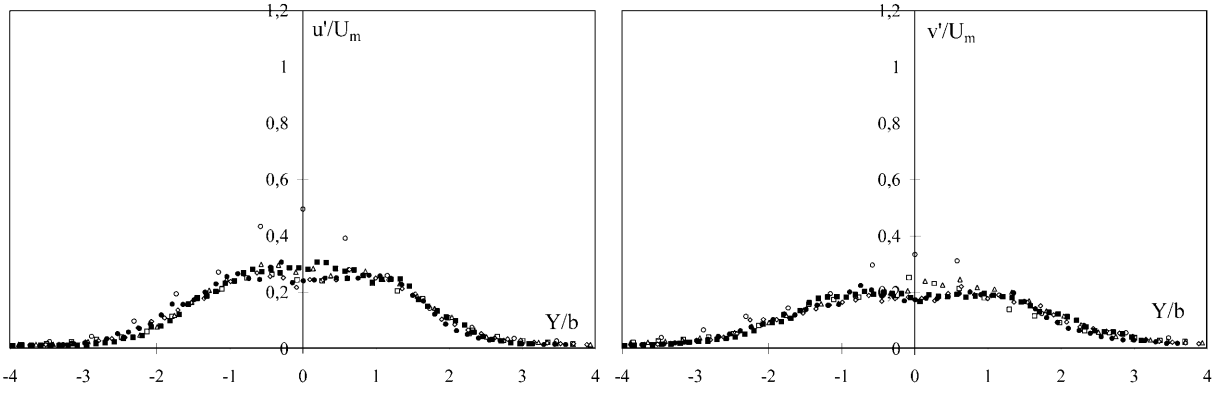

c) Purely alternating jet

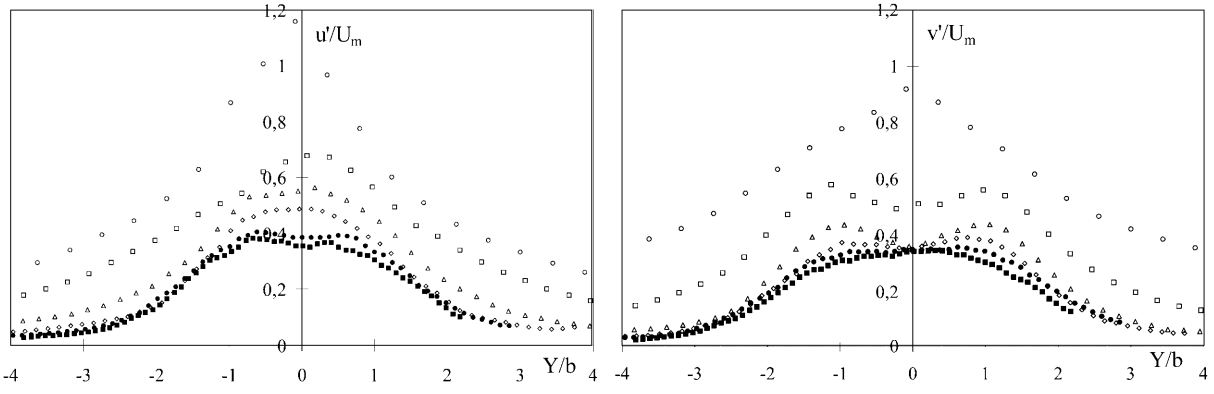

d) Mixed pulsed jet

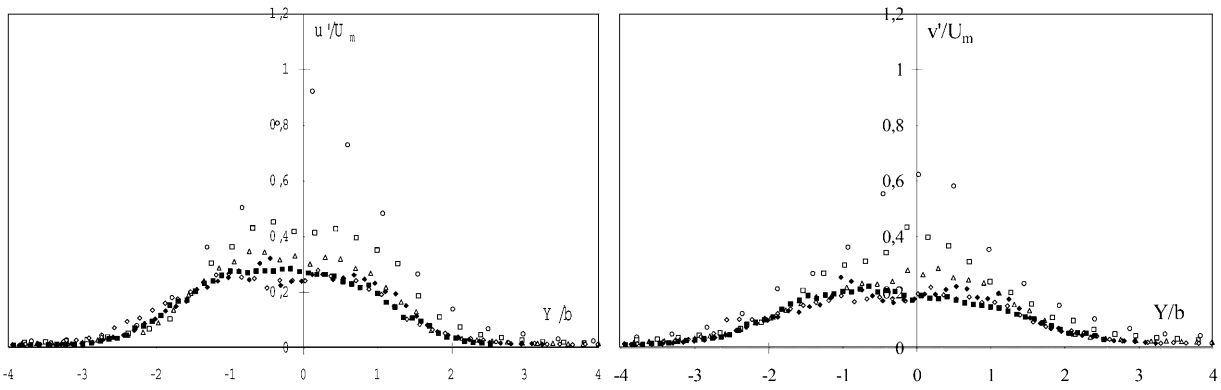

Fig. 10a–d. RMS velocity fluctuation normalized profiles, ○ $X/e = 5$, □ $X/e = 10$, Δ $X/e = 15$, ◇ $X/e = 20$, ● $X/e = 25$, ■ $X/e = 30$: **a** Steady jet (low level), **b** Steady jet (high level), **c** Purely alternating jet, **d** Mixed pulsed jet

5.2
Statistics of the vortex centers

The eddy structure centers obtained by the Γ-criterion presented in Sect. 2.3 can be localized on the phase-averaged velocity fields for every phase of the injection cycle. As an illustration, results are presented in Fig. 13 for the phases 0° and 180°. One can see the accuracy of the locations, hence enlightening the velocity fields plotted in Figs. 11 and 12.

An example of fluctuations of the vortex center around its 180° phase-average position is given in Fig. 14 for the purely alternating jet. At $X/e = 7$ the most recent vortex pair is clearly detected, with a small dispersion ($\sigma = 0.6$), permitting a meaningful phase-averaged position to be defined. The previous vortex pair is also visible around $X/e = 25$, but now with a large dispersion ($\sigma \approx 4$), which could be explained by vortex pair oscillations.

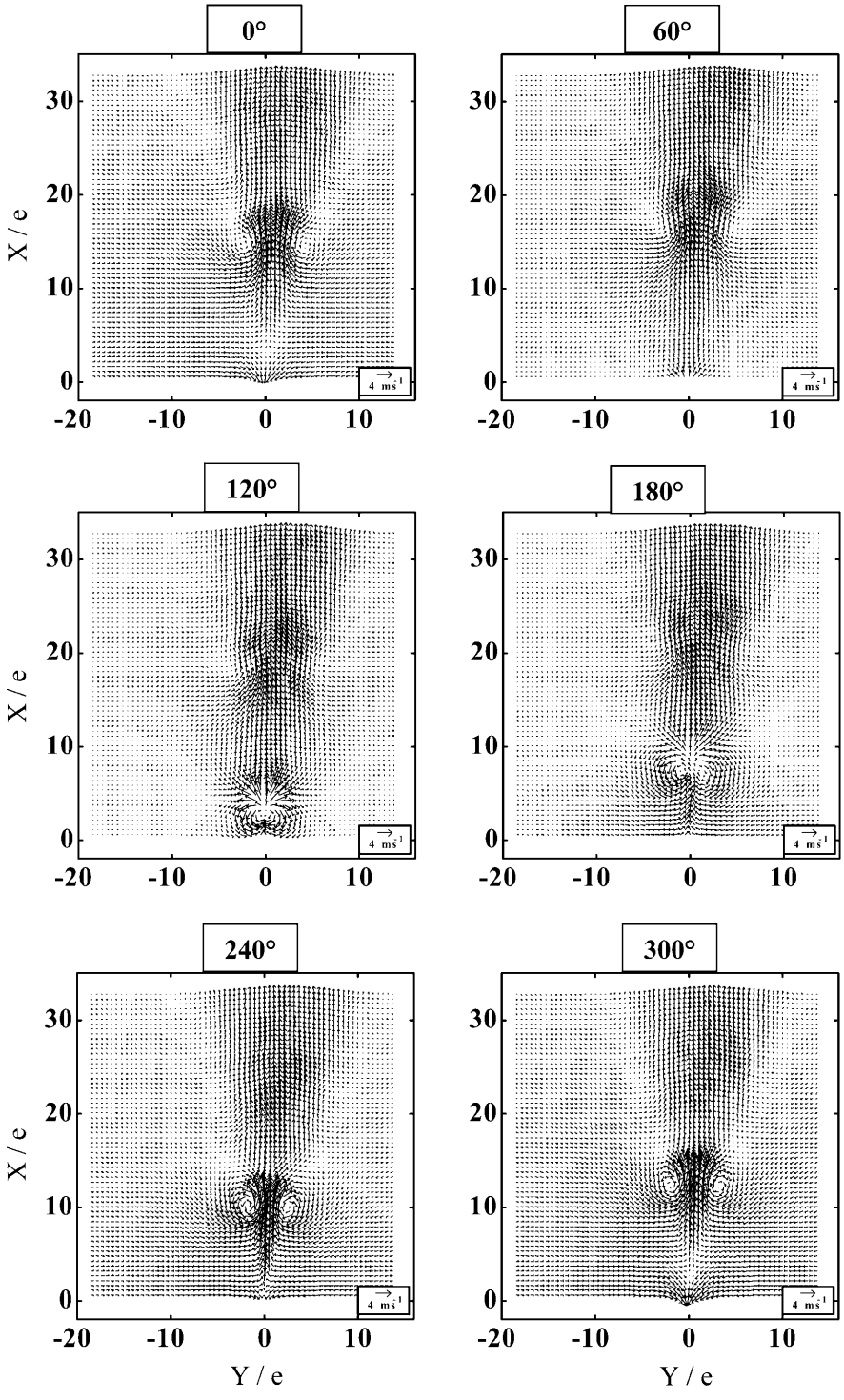

Fig. 11. Phase-average velocity fields for purely alternating jet at 60° intervals of the injection cycle

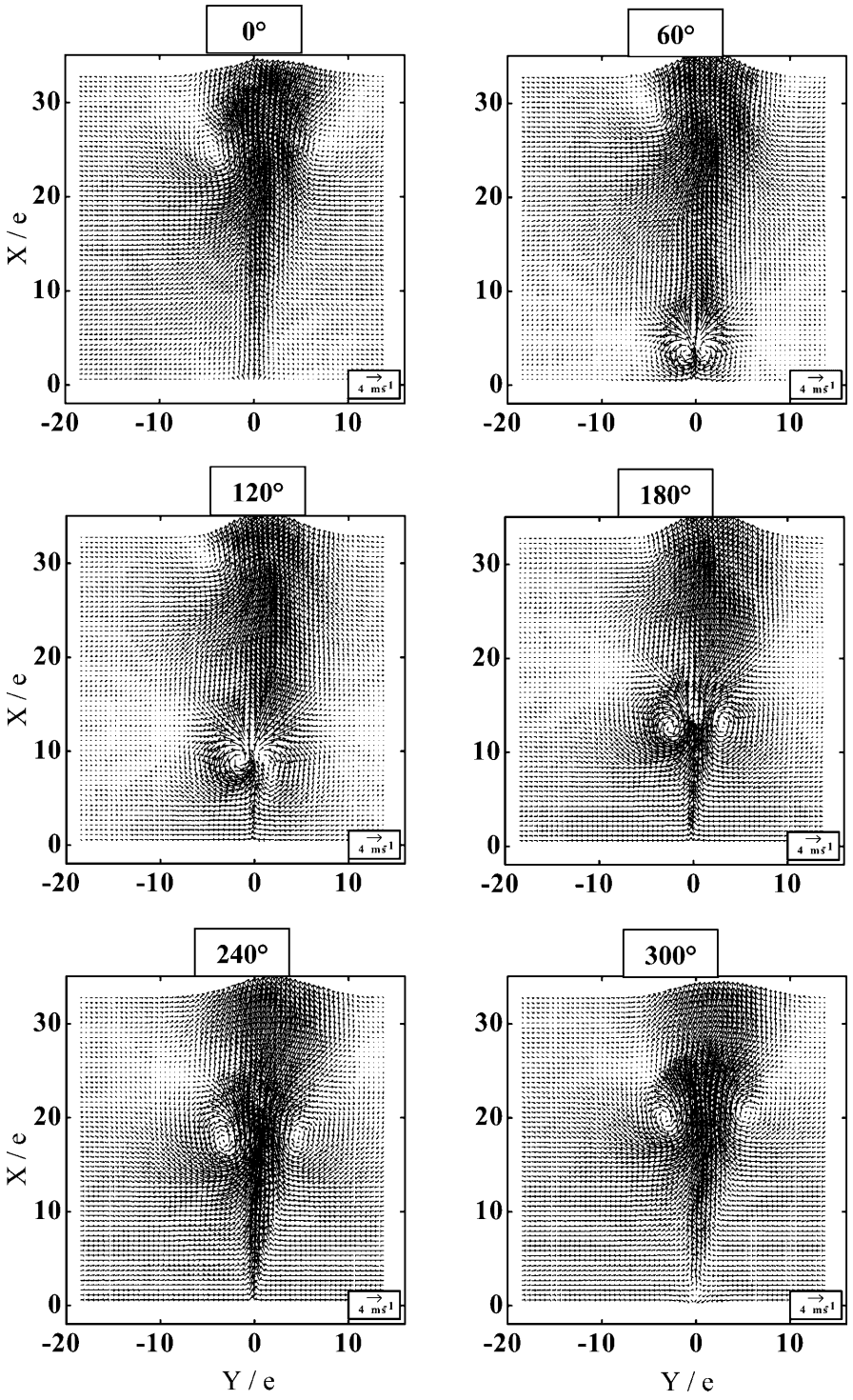

Fig. 12. Phase-average velocity fields for mixed pulsed jet at 60° intervals of the injection cycle

5.3
Trajectories of the vortex centers

Figure 15 shows the phase-averaged trajectories covered by the vortex centers in steps of 20° of phase-angle of the injection cycle. The convection velocity of the vortices can be deduced from their locations and the actuator frequency of 200 Hz. Neglecting the convection velocity differences between steps, the averaged longitudinal convection speed is around 3.5 m/s for the purely alternating jet and 5 m/s for the mixed jet. These velocities can be compared with the U_m values of Fig. 8. In particular, for the purely alternating jet, the vortex displacement velocity is slightly larger than U_m. This result shows that the contra-rotating eddies are not passively convected by the flow, but they really control the whole jet dynamics. The mean flow essentially results from the self-induced motion of the vortex pairs.

The trajectories are clearly not linear. At their beginning, they are roughly defined by approximately parallel vertical mean lines up to $X/e = 6$ from the slit: this corresponds to the stage of formation. The cross-stream distances between the two eddy centers are, however,

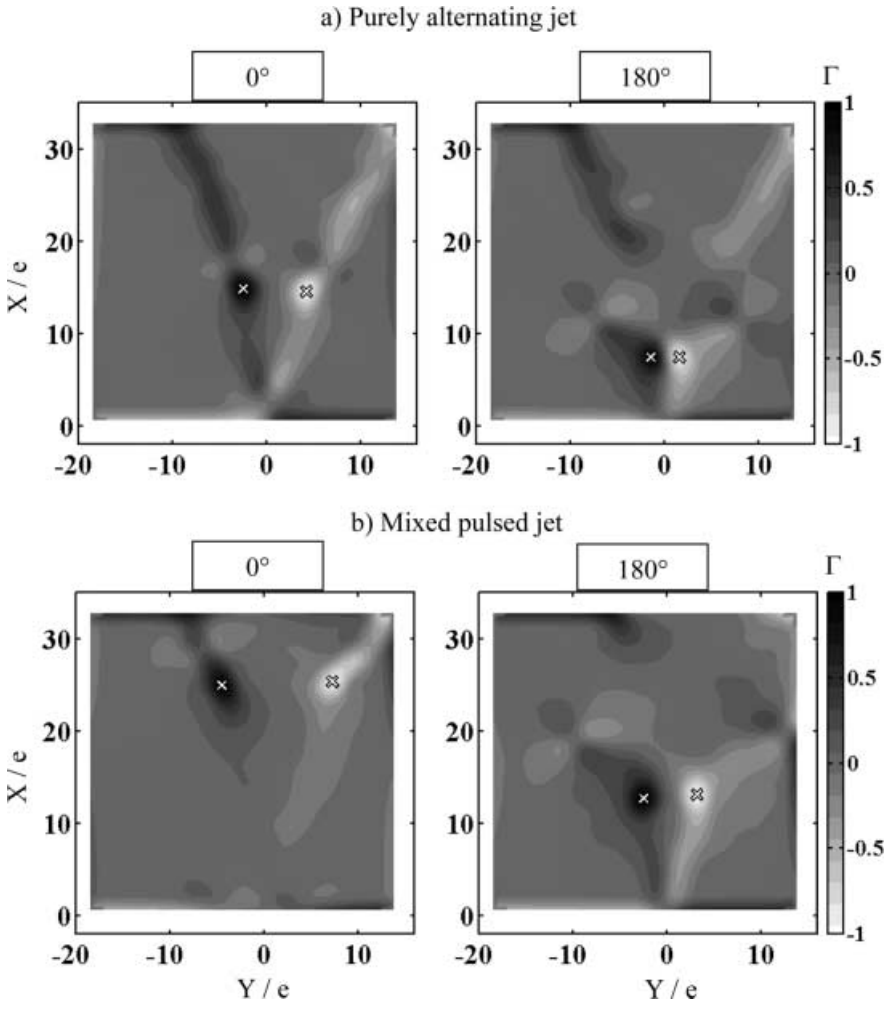

Fig. 13a–b. Γ-criterion maps for phase-average fields: **a** Purely alternating jet, **b** Mixed pulsed jet; on the left: at the phase 0° – end of suction, on the right: at the phase 180° – end of blowing. Eddy centers marked by crosses

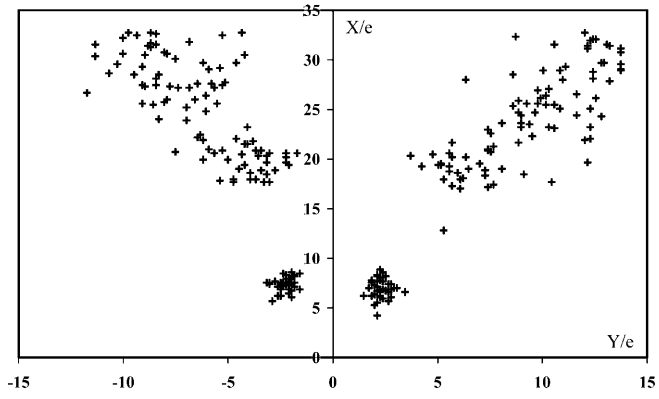

Fig. 14. Positions of the vortex centers for the 55 snapshots at phase 180° for purely alternating jet

slightly different between the purely alternating and mixed pulsed jets. Then, the two structures become larger and move away from each other: this corresponds to the stage of expansion. The lateral expansion angle is substantially greater for the alternating jet than for the mixed

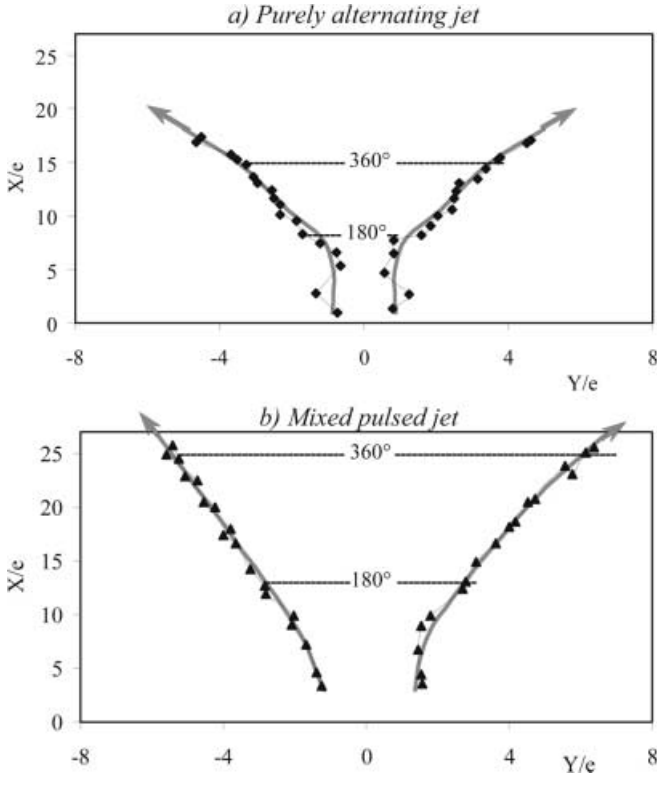

Fig. 15a–b. Positions of phase-average vortex centers at each 20° of the injection cycle (for phase definition, see Fig. 2): **a** Purely alternating jet, **b** Mixed pulsed jet

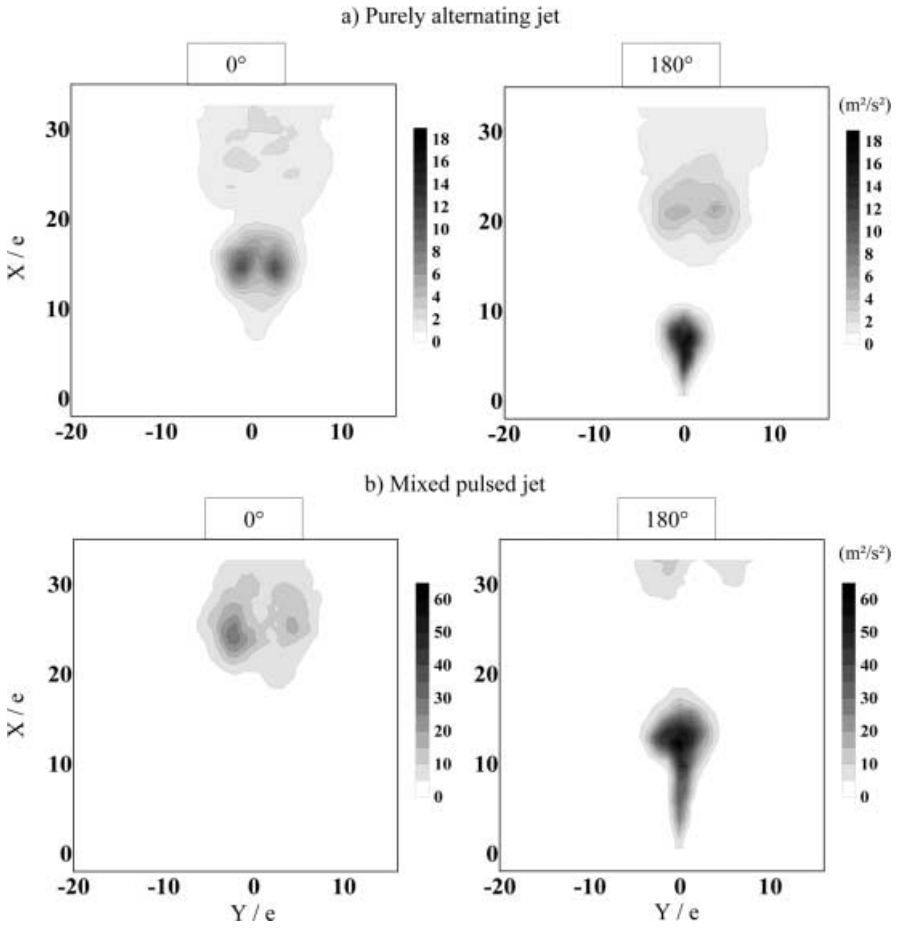

Fig. 16a–b. Energy of velocity fluctuations for synchronized fields: **a** Purely alternating jet, **b** Mixed pulsed jet; on the left: at the phase 0° – end of suction, on the right: at the phase 180° – end of blowing

jet, which is consistent with the half-width results given Fig. 7.

5.4
Velocity fluctuations around the phase averages

The velocity fluctuations around a phase-average field inside the synchronized series of instantaneous fields are now studied at the two important injection phases of 0° and 180°, Fig. 16. Comparisons with Figures 11, 12 or 15 show that the fluctuation maxima are located on the phase-averaged vortices. The kinetic energy is large, suggesting an irregular motion of these structures.

In addition, turbulence is present in the velocity field at specific times in the injection cycle. During the blowing phase (Fig. 16, right), there is turbulence in the wake of the rising structures – i.e. in the blowing jet itself. On the contrary, at the end of the suction phase (Fig. 16, left), there are no fluctuations close to the wall, in accordance with the laminar state of the sucked flow.

Two examples of instantaneous fields at a same phase are given in Fig. 17. They permit one to appreciate the differences that occur between realizations. In particular, we notice that the synchronized structures vary in intensity from one realization to another, and that the vortex pairs are generally not symmetrical. The most intense vortex structures can move toward the left or the right. As a result, the instantaneous jet deviates in a similar way. These findings, which disappear in any averaged view, will now be analyzed using POD.

The POD analysis was applied to each phase-locked series of instantaneous fields. For both the purely alternating jet and the mixed pulsed jet, the first mode corresponds precisely to the phase-averaged fields. All the upper modes are approximately symmetrical or antisymmetrical, corresponding to stream-wise jet oscillations or span-wise jet swings. Figure 18 shows the second mode (antisymmetric) at phase 0° of the injection process. For both jets, this mode is dominated by triplets of eddies, composed by two structures antisymmetric about the jet mid-plane (ccw on the maps) and surmounted by one contra-rotating structure (cw on the maps). These triplets, even less energetic than the first mode, react with it so as to deviate the phase-averaged structures, once to the left, once to the right, depending on the sign of the modal coefficient. The resulting effect will be a slight swinging of the jet, in accordance with the differences between the instantaneous fields presented in Fig. 17.

6
Conclusions

The present PIV investigation on a *purely alternating jet* with zero mass-flux and a *mixed pulsed jet* with an additional blowing component has shown that well-organized large flow patterns dominate the velocity fields by a periodic flux of contra-rotating eddy pairs. There is accordingly a large lateral expansion of the jet and a large entrainment rate of external fluid, compared to usual

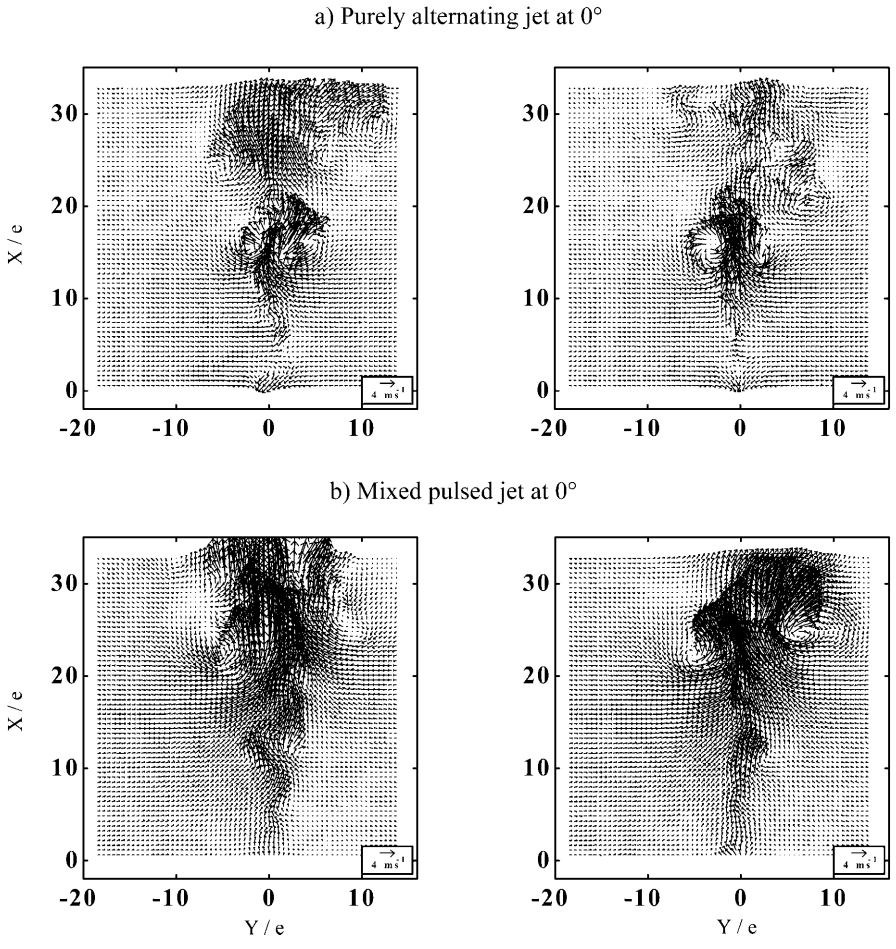

Fig. 17a–b. Examples of instantaneous velocity fields at the end of the suction phase (0°): **a** Purely alternating jet, **b** Mixed pulsed jet

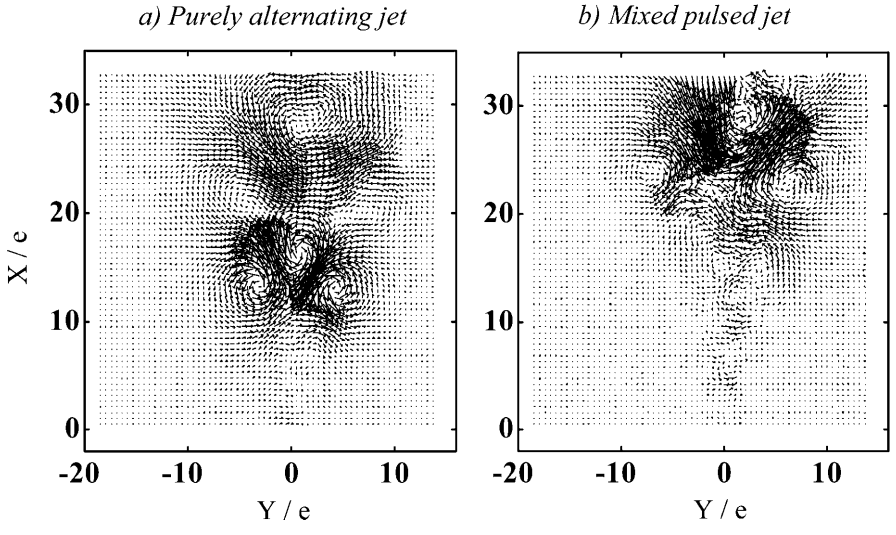

Fig. 18a–b. POD second mode for 0° phase-average velocity fields: **a** Purely alternating jet, **b** Mixed pulsed jet

steady jets. This property is basically linked to the self-induced convective motion of eddy pairs. The flow structures may vary significantly from one injection cycle to another, but phase-average eddies are well identified and can be traced over the whole injection cycle. The suction that exists close to the wall for these two types of pulsed jets is also well marked, being in particular largest for a purely alternating pulsed jet.

References

Amitay M; Honohan A; Trautman M; Glezer A (1997) Modification of the aerodynamic characteristics of bluff bodies using fluidic actuators. In: Proc 28th AIAA Fluid Dynamics Conference, Snowmass Village, USA

Ben Chiekh M; Béra JC; Michard M; Sunyach M (2000) Contrôle par jet pulsé de l'écoulement dans un divergent court à grand angle – Pulsed jet control of a short diffuser. C R Acad Sci Paris 328: 749–756

Béra JC; Sunyach M (1998) Control of boundary layer separation by jet oscillation. In: Proc 4th AIAA/CEAS Aeroacoustics Conference, Toulouse, France, June 1998, pp 967–973

Béra JC; Comte-Bellot G; Sunyach M (1998) Pulsed jet control of the turbulent boundary layer separation. C R Acad Sci Paris 326: 859–865

Béra JC; Michard M; Sunyach M; Comte-Bellot G (2000) Changing lift and drag by jet oscillation: experiments on a circular cylinder with turbulent separation. Eur J Mech 19: 575–595

Binder G; Favre-Marinet M; Kueny JL; Craya A; Laty R (1971) Jets Instationnaires, Laboratoire de Mécanique des Fluides, Université de Grenoble, France, October 1971

Binder G; Favre-Marinet M; Craya A; Te Veug Hac (1972) Jets Instationnaires, Laboratoire de Mécanique des Fluides, Université de Grenoble, France, June 1972

Bremhorst K; Harch WH (1979) Near field velocity measurements in a fully pulsed subsonic air jet. In: Durst F et al (eds) Turbulent shear flows, vol. 1. Springer, Berlin Heidelberg New York, pp 37–54

Bremhorst K; Watson RD (1981) Velocity field and entrainment of a pulsed core jet. J Fl Eng 103: 605–608

Chang Y; Vakili A (1995) Dynamics of vortex ring in crossflow. Phys Fluids 7: 1583–1597

Crow S; Champagne F (1971) Orderly structure in jet turbulence. J Fl Mech 48: 547–591

Curtet RM; Girard JP (1973) Visualization of a pulsating jet. Proc ASME Symp on the Fluid Mechanics of Mixing, Atlanta, pp 173–180

Getin N (2000) Simulation numérique du contrôle actif par jets pulsés de l'écoulement turbulent autour d'un cylindre circulaire. Ph. D. thesis, Ecole Centrale de Lyon, Ecully, France

Greenblatt D; Darabi A; Nishri B; Wygnanski I (1998) Separation control by periodic addition of momentum with particular emphasis on dynamic stall. American Helicopter Society, Gifu, Japan, April 1998, paper No T3–4

Hassan A; Janakiram R (1997) Effect of zero-mass "synthetic" jets on the aerodynamics of the NACA-0012 airfoil. In: Proc 28th AIAA Fluid Dynamics Conference, Snowmass Village, USA

Heywood JB (1988) Internal combustion engine fundamentals. McGraw-Hill

Kral LD; Donovan JF; Cain AB; Cary AW (1997) Numerical simulation of synthetic jet actuators. In: Proc 28th AIAA Fluid Dynamics Conference, Snowmass Village, USA

Kwong AHM; Dowling AP (1994) Active boundary layer control in diffusers. J AIAA 32: 2409–2414

Lee C; Goldstein D (2000) Two-dimensional synthetic jet simulation. In: Proc 38th Aerospace Sciences Meeting and Exhibit, Reno, USA

Mary I; Sagaut P; Guillen P (2000) Etude numérique du contrôle du décollement par simulation des grandes échelles. Technical report RTS 21/4368 DSNA/Y, ONERA, France

McManus K; Magill J (1997) Airfoil performance enhancement using pulsed jet separation control. In: Proc 4th AIAA Shear Flow Control Conference, Snowmass Village, USA

Michard M; Graftieaux L; Lollini L; Grosjean N (1997) Identification of vortical structures by non local criterion: application to PIV. Measurements on DNS-LES results of turbulent rotating flows. In: Proc 11th Symposium on Turbulent Shear Flows, Grenoble, France

Michard M; Béra JC; Sunyach M; Benarrous E; Grosjean N; Perrin JM; Safsaf D; Roland P (1998) Etude aérodynamique expérimentale relative au contrôle du décollement par jets pulsés. Contract report ONERA/METRAFLU 23.251/DA.B1/DC

Rediniotis OK; Ko J; Yue X; Kurdila AJ (1999) Synthetic jets, their reduced order modeling and applications to flow control. In: Proc 37th AIAA Aerospace Sciences Meeting and Exhibit, Reno, USA

Rizzetta D; Visbal M; Stanek M (1998) Numerical investigation of synthetic jet flowfields. Albuquerque, USA

Seifert A; Bachar T; Koss D; Shepshelovich M; Wygnanski I (1993) Oscillatory blowing: a tool to delay boundary-layer separation. J AIAA 31: 2052–2060

Sirovich L (1987) Turbulence and the dynamics of coherent structures, Part I: Coherent structures. Quarterly of Appl Math 45: 561–571

Smith BL; Glezer A (1998) The formation and evolution of synthetic jets. Phys Fl 10: 2281–2297

Smith BL; Trautman MA; Glezer A (1999) controlled interactions of adjacent synthetic jets. In: Proc 37th AIAA Aerospace Sciences Meeting and Exhibit, Reno, USA

Wygnanski I (1997) Boundary layer and flow control by periodic addition of momentum. In: Proc 28th AIAA Fluid Dynamics Conference, Snowmass Village, USA